Understanding groundwater salinization mechanisms to secure freshwater resources in the water-scarce city of Maputo, Mozambique

G. Nogueira.[1,2]; T. Y. Stigter[2]; Y. Zhou[2]; F. Mussa[3]; D. Juizo[3]

[1]*Present address: Helmholtz-Zentrum für Umweltforschung, Department of Hydrogeology, 04318 Leipzig, Germany*
[2]*IHE Delft Institute for Water Education, Department of Water Science and Engineering, 2611 AX Delft, the Netherlands*
[3]*Universidade Eduardo Mondlane, Department of Engineering, 3453 Maputo, Mozambique*

Corresponding author: *guilherme.nogueira@ufz.de*

Reference to this article:
https://doi.org/10.1016/j.scitotenv.2018.12.343 -0048-9697/

Abstract

In this study hydrochemical, isotopic and multivariate statistical tools are combined with a recharge analysis and existing geophysical data to improve understanding of major factors controlling freshwater occurrence and the origins of high salinities in the multi-layered coastal aquifer system of the Great Maputo area in Mozambique. Access to freshwater in this semi-arid area is limited by an inefficient public supply network, scarce surface waters, long droughts and an increasing population growth. Groundwater has a large potential to enhance water security, but its exploitation is threatened by both coastal and inland salinization mechanisms that are poorly understood. A GIS approach is utilized to classify potential recharge zones based on hydrogeological properties and land use/cover, whereas potential recharge rates are estimated through a root zone water balance method. In combination with water stable isotope data results reveal that extreme rainfall events provide the most relevant contributions to recharge, and interception and evaporation play an important role in the low recharge areas. Hierarchical clustering of hydrochemical and isotopic data allows the classification of six water groups, varying from fresh to brackish/salt waters. Corresponding scatter plots and PHREEQC modelling show

evaporation and mixing with seawater (up to 5%) as major processes affecting salinity in the area. The co-occurrence of high alkalinity and Cl concentrations, in combination with piezometric and geo-electrical data, suggests that: 1) inland brackish/salt groundwater is caused by mixing with seawater trapped within clay layers; and 2) brackish/salt surface waters result from seepage of brackish groundwater into rivers and wetlands, followed by evaporation, hence increasing salinity and $\delta^{18}O$ values. Mixing with small fractions of trapped seawater as main salinity source, rather than halite dissolution, is further corroborated by Br/Cl ratios of brackish/salt water samples near the ocean ratio. Cation exchange upon salinization is mainly observed in the semi-confined aquifer, while freshening takes place in the phreatic aquifer, particularly in areas presenting high recharge rates.

Keywords

Saltwater intrusion; old trapped seawater; evaporation; extreme rainfall recharge; hydrochemistry; semi-arid coastal aquifer

1. Introduction

Rapid population growth and social-economic development increase water demand across the globe, in particular for agriculture and human consumption. However, in various places, among which poor semi-arid regions, surface water resources are scarce or of undesired quality, which increases the pressure on local groundwater resources (Edmunds et al., 2006; Werner et al., 2013). Moreover, coastal groundwater resources are expected to suffer the largest impacts due to high and increasing population density, with more than one billion people currently living near shoreline areas (Ferguson and Gleeson, 2012). In addition, studies from Werner et al. (2013) and Neumann et al. (2015) show that climate change effects, such as increasing temperatures, more frequent droughts and sea level rise, amplify the risk of degradation of coastal aquifers caused by human activities. In this context, adequate knowledge of coastal

groundwater systems and the controlling physical and chemical processes is crucial for their sustainable management, which implies optimizing their use and minimizing negative side effects such as over-exploitation and saltwater intrusion. Notwithstanding, salinization mechanisms in semi-arid coastal aquifers can have diverse origins, occurring alone or concomitantly, with dominant mechanisms described as:

- seawater intrusion: when pumping activities are uncontrolled and/or too close to the shoreline the naturally occurring fresh/saltwater interface can migrate inland (e.g. Barlow and Reichard, 2010; Ferguson and Gleeson, 2012; Post, 2005; Vengosh et al., 2002; Werner et al., 2013) this process is well-known and widely documented as the major issue in coastal water resource management;
- dissolution of evaporites (Chi and Savard, 1997; Güler and Thyne, 2004; Heston, 2015): minerals such as halite (NaCl) and gypsum ($CaSO_4.2H_2O$) are highly soluble when in contact with water and their dissolution may lead to extremely high salinities caused by the release of these ions into water (e.g. Bouchaou et al., 2008; El Yaouti et al., 2009; Han et al., 2013; Mongelli et al., 2013);
- presence of connate saltwater or trapped seawater related to earlier transgression periods: usually within clay and silt formations, or at the bottom of aquifer formations, due to its higher density, although also found in shallower layers of aquifers due to poor flushing (freshening) capacity, or due to disturbance of the system by pumping activities (e.g. Bouchaou et al., 2008; Currell et al., 2015; Hiscock and Bense, 2014; Lee et al., 2016; Mollema et al., 2013);
- agricultural return flow: solutes are concentrated by strong evapotranspiration and recycling of water; in such cases nitrate (NO_3^-) is typically found in high concentrations due to flushing of fertilizers, if the environment is aerobic (e.g. Andrade and Stigter, 2009; Currell et al., 2010; Edmunds et al., 2006; Steinich et al., 1998; Stigter et al., 1998; Trabelsi et al., 2007; Zghibi et al., 2013).

The diversity of potential diffuse and point sources of salinity requires a good understanding of the hydrogeological context of the area, the local recharge processes and hydrogeochemical processes, as

well as a good set of analysis tools to determine controlling salinization mechanisms. Works from Martinez et al. (2017), Güler and Thyne (2004) and Swanson et al. (2001) have shown the combined application of modelling, multivariate statistical techniques, hydrochemical indicators and isotopes to characterize fresh, brackish and saline waters, their origin and evolution. One such hydrochemical indicator is bromide (Br^-), widely applied to help distinguish salinity origins (Alcala and Custodio, 2008; Chi and Savard, 1997; Han et al., 2013, 2011; Iverach et al., 2017; Lee et al., 2016; Mollema et al., 2013; Mongelli et al., 2013). There is still further need for comprehensive assessments of hydrochemical evolution and salinization mechanisms at the local to regional scale, for two main reasons: i) to enhance the knowledge and understanding of the heterogeneity and complexity of saltwater intrusion in different climate and hydro(geo)logical settings; ii) to correctly target specific mitigation measures (reducing salinity) and/or adaptation measures (using brackish water). Since the 1990's the Maputo province in Mozambique is experiencing some of the highest population growth rates in the country (2.5% per year, United Nations, 2017), expanding from 2 million people in 2007 to about 2.5 million people in 2017 (Rosário Dias, 2016). As surface water resources are limited and threatened by typical long drought periods, groundwater complements local water supply, which raises concerns about the water quality and possible aquifer depletion. Brackish/salt groundwater (electrical conductivity (EC) between 4000 and 9000 µS/cm) has been previously documented as a limiting factor for groundwater use in the inland sectors of the semi-confined aquifer and in the north of the study area (BURGEAP, 1962; Chairuca et al., 2016; DNA, 1988; Matsinhe et al., 2008; Muiuane, 2007; Smidt, 1990). Notwithstanding, the main origins of such saltwater occurrence were unclear prior to the current study. In this regard, the current study aims to demonstrate the successful application of a multi-method approach within the specific climatic and geographical setting of an African semi-arid coastal aquifer, involving (i) recharge assessment, (ii) geological and geophysical information analysis, and (iii) an in-depth hydrochemical and stable isotopic research.

2. Study area

The study area is located in the south of Mozambique, in the Maputo Province (Fig. 1), covering an area of approximately 6300 km^2. Maximum elevations are around 230 *masl* in the westernmost area, but overall the topography is rather flat, consisting of gentle slopes (0 - 10 degrees) with rare exceptions close to river valleys and hills (Fig S.1 in supplementary material). The climate in the area is characterized as savanna, resembling a semi-arid environment with slightly higher precipitation rates (Kottek et al., 2006; Muiuane, 2007). Mean annual precipitation ranges from 400 to 800 mm/year (average of 700 mm/year), while mean potential evapotranspiration (ETP) is much higher, between 1000-1500 mm/year (Rosário Dias, 2016). Natural herbaceous vegetation and shrublands form the main land use/cover in the region (FAO, 2015). Apart from small-scale agriculture, vast sugar-cane plantations exist in the north of the area, which are mostly fed by rain and additional irrigation from surface water (HYDROCONSEIL/WE-Consult, 2011) (Fig S.1).

Surface water resources are scarce in the area (Fig. 1). The Incomati River constitutes the largest source and presents mainly fresh and unpolluted waters. It is extensively exploited for small-scale agriculture and sugar-cane irrigation in its upstream areas (Adonis, 2007). The Matola River is a perennial river that consists of mostly brackish/salt water originating from groundwater seepage, as will be shown in this study. In addition, EC values up to 40 mS/cm have been recorded near the river mouth and are mainly attributed to surface seawater incursion (FIPAG et al., 2012; Rosário Dias, 2016; Smidt, 1990).

At the scale of this study two main aquifers are defined in the area: an unconfined (or phreatic) aquifer and a semi-confined aquifer. The first is found within the Quaternary aeollian sand deposits, and the second within consolidated sands, sandstones and carbonate rocks (mostly calcarenites) from the lower Cenozoic (Salman and Abdula, 1995; Smidt, 1990). Previous studies suggest thicknesses of 5 to 50 m for the phreatic aquifer, and 50 to 60 m for the semi-confined aquifer (Fig. 1). The aquifers are connected

through an aquitard unit made up of silty marl and clay. In some areas this formation is very thin (< 2m thickness) or absent, so that the system can be analysed as a single unit (Chairuca et al., 2016; DNA, 1988; IWACO, 1986; Juizo, 1995; Matsinhe et al., 2008; Muiuane, 2007), further revealed by a small hydraulic head difference between shallow and deep wells (< 10 cm). Basalts and rhyolites related to the Jurassic rift sequence can be observed at the Western boundary of the study area.

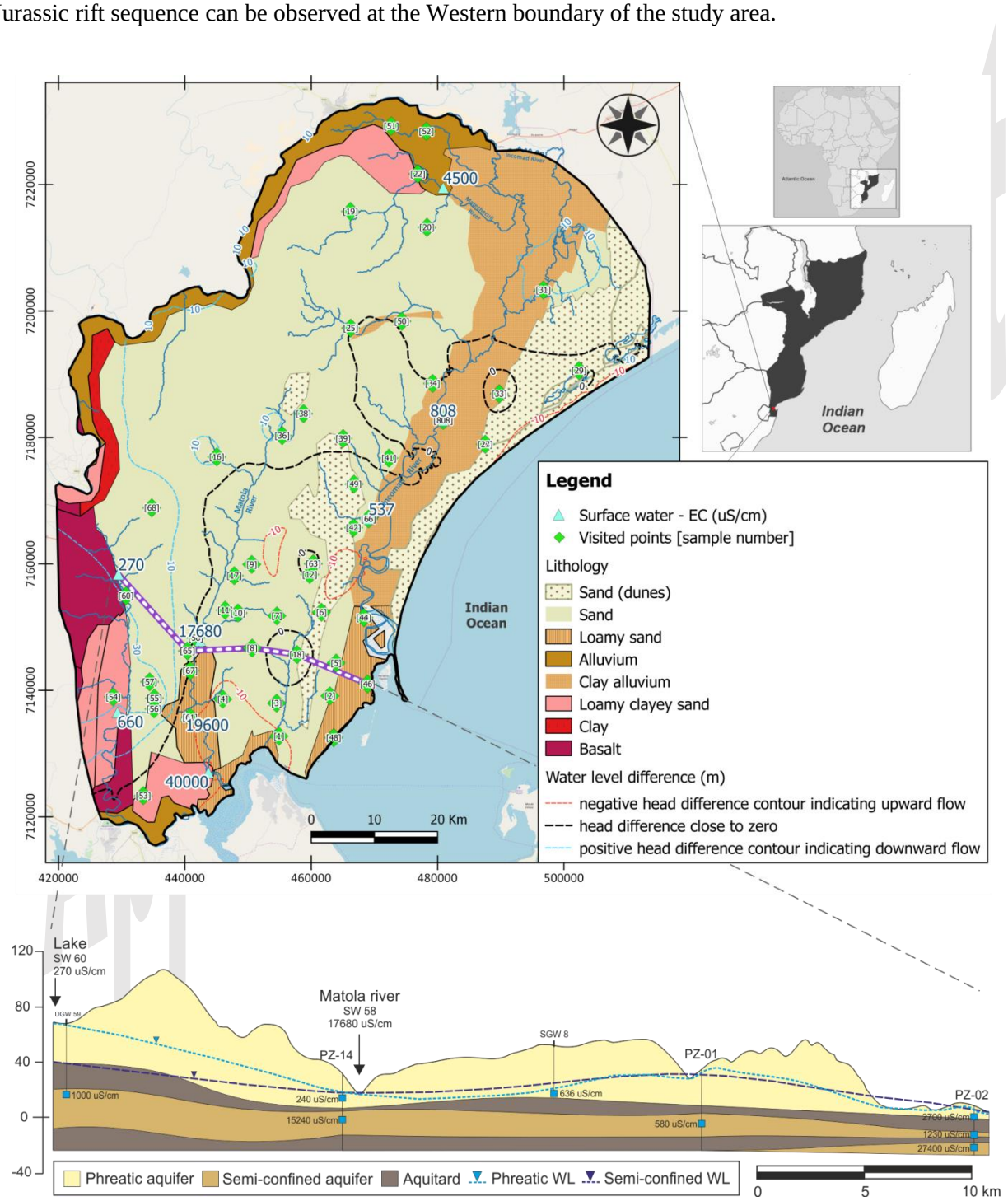

Fig. 1: Location map and geological context of the study area, together with sampled points, surface water EC values, and calculated groundwater head differences between the phreatic and semi-confined aquifers in May 2017. A cross section view of the area is presented on the bottom of the figure (purple line on the map) together with interpolated hydraulic heads, field EC measurements and sample depths. Note the vertical exaggeration of the profile. Mind that the cross-section view is slightly oblique to main groundwater flow. **(2 column fitting image, color)**

The hydraulic properties of the aquifer vary depending on the local lithological setting. Currently, only transmissivity values for the unconfined aquifer near Maputo City are available, estimated between 200 - 400 m^2/day, and up to 1600 m^2/day in wells with thick coarse sands (HYDROCONSEIL/WE-Consult, 2011; IWACO, 1986). Groundwater levels range from 60 to 2 *masl*, with the highest hydraulic heads in the phreatic aquifer on the western hills (Fig. 1). Natural groundwater recharge ranges between 5% and 30% of total annual rainfall, depending on soil type and vegetation cover, as will be discussed in this paper. In drier areas covered by low permeability soils, recharge rates can be as low as 10 mm/year (Chairuca et al., 2016; DNA, 1988).

3. Materials and methods

3.1 Data collection and sample analysis

Hydrogeological investigation and technical reports from ARA-Sul, HYDROCONSEIL/WE-Consult (2011) and IWACO (1986) were assessed for primary data collection and current understanding of the local hydrogeology, as well as for collection of existing groundwater levels. Climate data were acquired from local meteorological stations and land use/cover data from FAO (2015).

Surface water and groundwater samples were collected from streams and monitoring and pumping wells during a field campaign held in April/May 2017. The selection of sample sites was constrained by well availability and access, while aiming for the best coverage and representativeness of the area. A total of

67 groundwater samples and 5 surface water samples were collected for major cations (Na^+, K^+, Mg^{2+}, Ca^{2+}) and anions (Cl^-, HCO_3^-, SO_4^{2-}, NO_3^-), and water stable isotopes (^{18}O and ^2H) analyses. Additionally, 17 unfiltered samples were collected for Br^- analyses at locations where measured EC was higher than 1500 µS/cm, and also at few locations with low EC to get an idea of background values in freshwaters. Field parameters including water level, EC, temperature and pH were measured during sampling with the Solinst 107 TLC meter, a Greisinger portable digital Conductivity meter, and a WTW pH meter, respectively. For alkalinity, unfiltered samples were titrated with the HACH Digital Titrator titration field kit. We assumed alkalinity as being the acid-neutralizing capacity of total solutes and particulates, since the expected titratable particulate matter is very low in the majority of collected samples.

All samples were stored at 4 °C until they were analysed in the lab. Samples for cation analysis were stored in pre-acidified polyethylene bottles (HNO_3 10%). Major cations and anions were analysed at the laboratory of IHE Delft following standard procedures, through Inductively Coupled Plasma Mass Spectrometry (ICP-MS) and Ion Chromatography System (ICS), respectively. Lab results were checked through ion error balance (Appelo and Postma, 2005; Hiscock and Bense, 2014) and samples presenting absolute ionic error (IE) above 10% were excluded from analysis. Stable isotope analyses were also performed at the laboratory of IHE Delft using a liquid-water isotope analyser (LGR) (accuracy of ±0.2 ‰ for $\delta^{18}O$ and ±0.6 ‰ for δ^2H). Results are reported as parts per thousand (‰) with respect to Vienna Standard Mean Ocean Water (VSMOW) using the standard δ notation (Mook, 2001; Rozanski et al., 2001). Br^- was analysed through a high-resolution Ion Chromatography (IC) at ActLabs (Toronto, Canada). Mineral saturation indices (SI) were calculated in PHREEQC, which was also used for specific hydrochemical modelling.

3.2 HCA and hydrochemical analysis

Water types were classified according to the Stuyfzand system (Stuyfzand, 1989), considering Cl^- concentration, alkalinity as HCO_3^-, and the major cation and anion. It is a well-known classification system and widely applied in hydrochemical studies in coastal and semi-arid regions (e.g. de Louw et al., 2010; Giménez et al., 2010; Giménez and Morell, 1997; Marconi et al., 2011; Mollema et al., 2013; Vandenbohede and Lebbe, 2012).

Samples were divided in water groups with support of Hierarchical Cluster Analysis (HCA), a multivariate statistical technique for grouping large data sets into subgroups (or clusters). HCA depicts correlation patterns among the water samples and thus allows a swifter identification of the main hydrochemical processes than when only descriptive statistics are used (Andrade and Stigter, 2011; Güler and Thyne, 2004). For HCA, the cluster analysis module from the software "IBM SPSS Statistics 20" was used considering 13 variables (EC, pH, Na^+, K^+, Mg^{2+}, Ca^{2+}, Cl^-, HCO_3^-, SO_4^{2-}, NO_3^-, Na/Cl, SO_4/Cl, $\delta^{18}O$), following a number of trials and based on previous experiences. Parameters presenting a skewed distribution were log-transformed and standardized prior to HCA. Ward's method (Ward, 1963) for linkage was applied in accordance with other authors (e.g. Andrade and Stigter, 2011; Ghesquière et al., 2015; Güler and Thyne, 2004), while a City Block Distance (CDB) was chosen instead of Euclidean distance for similarity measurement. According to Krause (1987) large variable differences are dampened with CDB, so other parameters play a bigger role in the clustering, avoiding excessive relevance of a parameter and deriving results similar to those using the Euclidean distance. Clustering can be further supported by statistics and graphical analyses, leaving it to the researcher's judgement to decide what the best position of the so-called *phenon line* is to separate the groups, depending on the research goals and related uncertainties (Kovács and Erőss, 2017).

The obtained water groups were interpreted in relation to hydrogeological, climate and land use characteristics. Identification of geochemical processes was further complemented with the help of scatter plots of relevant physicochemical parameters and conservative mixing models.

3.3 Recharge assessment

Groundwater recharge was assessed using a two-step approach (Nogueira, 2017). First a 'Geographical Information System Multi Criteria Decision Analysis' (GIS-MCDA) was used to delineate recharge zones based on four parameters: lithology, land use/cover, slope and drainage frequency (Fig. S1 in supplemental material). The parameters were weighted using a multi-influence-factor (Magesh et al., 2012), giving different weights to each parameter according to their interrelation and their influence on groundwater recharge. Further, different parameter classes (e.g. soil types, land use/cover) were scored according to their influence on recharge, with greater positive contribution resulting in higher scores. The scores were normalized (between 1 and 0) to avoid overestimation. The methodology is similar to other studies applying GIS techniques for recharge assessment and detailed descriptions can be found in Bonilla Valverde et al. (2016), Cherkauer (2003) and Shaban et al. (2006). Subsequently, the root zone water budget method (Haberle and Svoboda, 2015; Healy, 2010) was applied to each of the units defined with GIS-MCDA, considering soil parameters (specific yield, wilting point, extinction depth and runoff threshold), crop characteristics (crop factor and rooting depth), groundwater depth and climate data (precipitation and potential ETP), to compute groundwater recharge (in addition to actual evapotranspiration, runoff and change in soil storage) at a daily time-step for 10 years (2000-2010). The procedure is described in detail in Nogueira (2017).

4. Results

4.1 Delineation of recharge zones

The combination of the four selected criteria influencing groundwater recharge resulted in five categories of recharge potential (RP), from very high to very low (Fig. 2). Nearly 27% of the study area's surface presents a very high RP and 46% reveals a high RP. As expected, sand dunes covered by open shrublands have the highest RP, whereas the lowest RP is found within agricultural fields and clayey valleys. As stated by Bonilla Valverde et al. (2016) RP maps serve as a tool in supporting managed aquifer recharge site selection, depicting optimum places with higher potential for mitigation measures to increase groundwater recharge, while giving additional insights into natural recharge processes and their spatial distribution.

Recharge rates show great variation in the area, between 5% and 30% of monthly precipitation, with higher rates found within higher RP zones (Table S.1 in supplementary material). The results are in line with previous assessed values of around 20% (DNA, 1988; IWACO, 1986). A general pattern of high recharge between November and March is observed, coinciding with wet season in the area (Nogueira, 2017) (see also Fig. S.1 in supplementary material). To a certain extent shallow groundwater samples collected in areas with lower RP (Incomati River valley, urban areas in the south) present higher EC and an enriched isotopic composition in comparison to samples collected in high RP areas (Fig. 2).

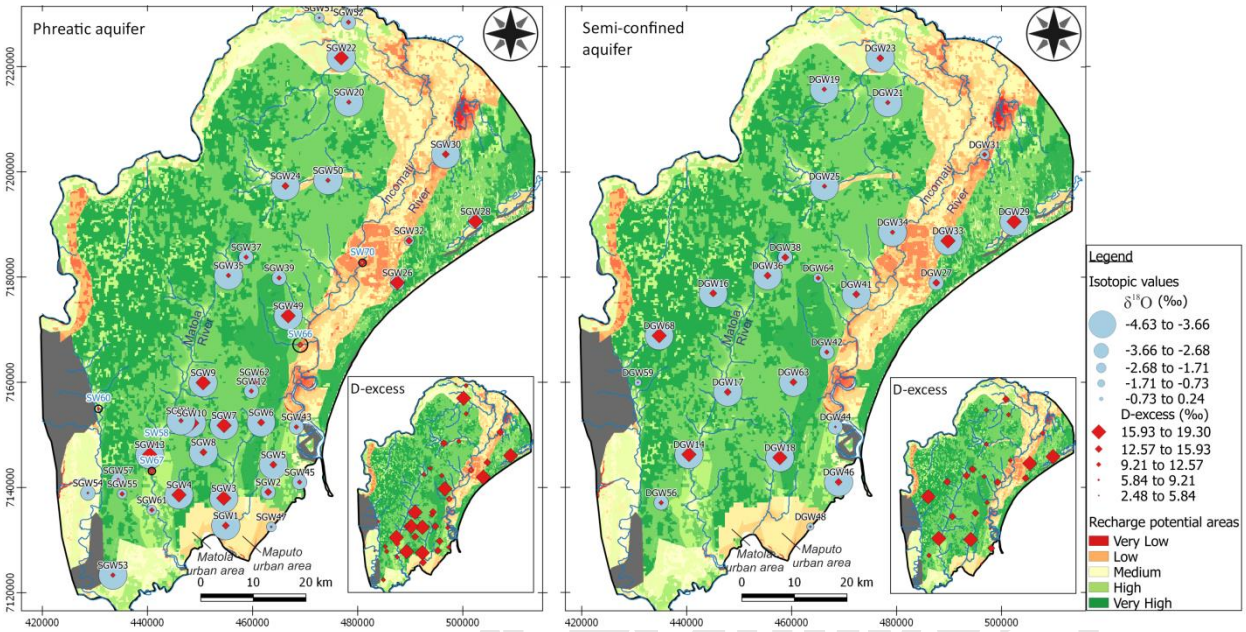

Fig. 2: Distribution of $\delta^{18}O$ and computed Deuterium excess (D-excess) of collected samples for both aquifers, together with RP map resulting from integration of four thematic layers (lithology, land use/cover, drainage frequency, slope). **(2 columns fitting image, color)**

4.2 General hydrochemistry

Descriptive statistics of main physico-chemical parameters of collected samples are presented in Table 1. A total of 66 samples, among surface and groundwater samples, were further analysed, as their absolute ionic error (IE) was below 10% (13 samples presenting IE between 5% and 10% were included but analysed with caution). Salinity, represented by EC, shows a large range in values (53.7 - 17,680 µS/cm; σ = 2,983 µS/cm). This large range is further reflected in the large standard deviations of major ions and anions. Values of pH are between 4.7 and 9.3, but for most samples between 6 and 8, indicating a near-neutral environment, but with significant differences between sampled groundwater environments. NO_3^- concentrations are generally low, with a few exceptions below the urban area of Maputo; all values are below the 50 mg/l drinking water guideline threshold for human consumption (WHO, 2011).

Table 1: Descriptive statistics of main physico-chemical parameters of collected water samples from the Great Maputo area. Solutes are presented in meq/l. Values below detection limit are expressed as <*d.l.*

The correlation among physico-chemical parameters is presented according to Spearman's rank as supplementary material in Table S.2. Very high correlations (≥ 0.80) are observed between Cl^- and Na^+, Cl^- and Br^-, Na^+ and Mg^{2+}, Sr^- and Br^-, and Sr^- and Cl^-, suggesting these elements have similar origins. Na^+ (0.78) and Ca^{2+} (0.71) also show significant correlation to HCO_3^-.

4.3 Water sample grouping (HCA)

HCA resulted in six main water groups (WT), presented in the dendogram of Fig. 3 together with a Stiff diagram of the average composition of each group. The clusters vary from fresh (WT-1, WT-2 and WT-3) to brackish/salt waters (WT-4, WT-5 and WT-6). The positioning of the phenon line in the dendrogram initially resulted in five groups. In an additional step WT-2 and WT-3 were "declustered" one order below the original position of the phenon-line, due to the relevant differences in salinity between the samples of these two groups, as well as the underlying hydrochemical processes. The characteristics and main physico-chemical parameters for each WT are presented in Table 2.

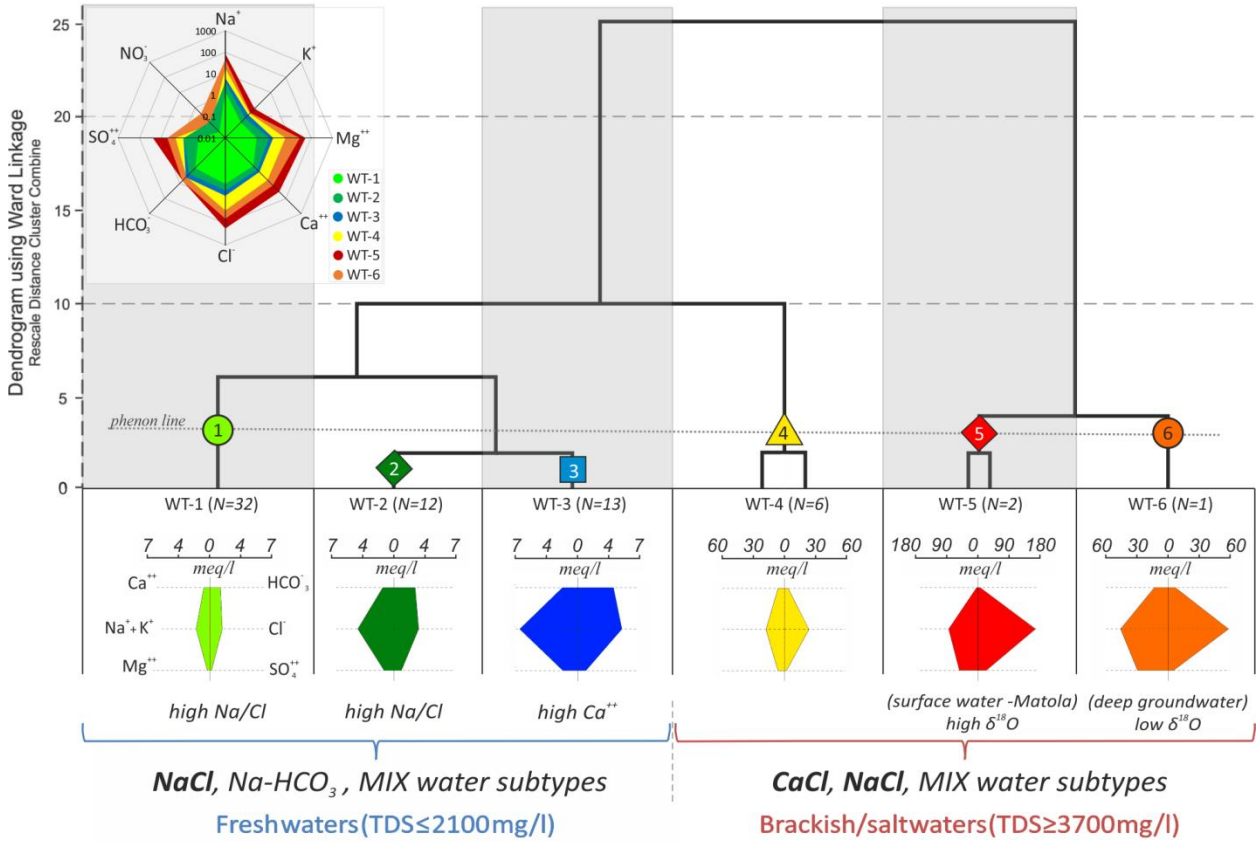

Fig. 3: Dendogram resulting from HCA and Stiff diagrams (meq/l) based on mean values of each water group. Number of samples for each WT is presented in brackets. Two major groups are defined according to TDS (mg/l) as freshwaters and brackish/salt waters. Note the different scales of the Stiff diagrams. The spider chart on the top presents mean concentrations of major ions and anions for each WT in meq/l. **(2 columns fitting image, color)**

Table 2: Main physico-chemical parameters and characteristics of water groups. Mean values are presented in brackets.

Most samples fall within freshwater water groups WT-1, WT-2 and WT-3 (57 out of 66 samples). These present low Cl^- concentrations and high Na/Cl ratios, both increasing from WT-1 to WT-3. On the contrary, brackish/salt water samples (WT-4, WT-5 and WT-6) present high EC and high Cl^- concentrations, with Na/Cl ratios generally below the ocean water ratio of 0.86. WT5 representing surface

water samples from the Matola River has the highest EC. Alkalinity shows an increasing trend from WT-1 to WT-6, but also has large variations within each WT; the saturation index (SI) with respect to calcite is mostly undersaturated in WT-1 and WT-2.

The water stable isotope distribution of the samples is shown in Fig. 4 together with the Global Meteoric Water Line (GMWL) from Craig (1961), and a Local Meteoric Water Line (LMWL) from Steinbruch and Weise (2016), computed as $\delta^2H=8.7*\delta^{18}O+15.5$ and based on rainwater samples taken in Mozambique, though quite far away from the study area. Four additional rainfall samples collected during field campaign are also included in the plot.

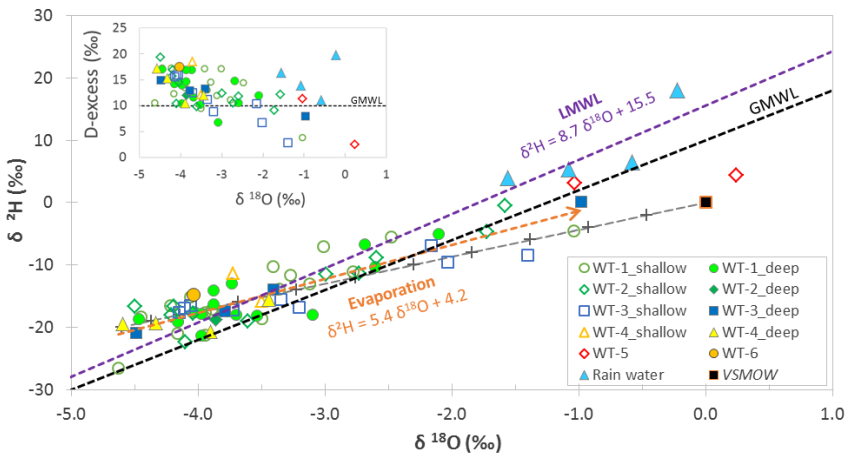

Fig. 4: Plots of δ^2H (D) *vs.* $\delta^{18}O$ (large plot) and D-excess versus $\delta^{18}O$ (small plot, both in ‰ in relation to VSMOW); groundwater samples are labelled as WT and rainfall samples are shown as blue triangles; also shown are the GMWL (dashed black line) from Craig (1961), the LMWL (dashed purple line) from Steinbruch and Weise (2016), the conservative mixing between VSMOW and freshwater end members (dashed grey line, each mark represents a 10% increase in seawater contribution) and the groundwater samples regression line (orange line, R^2=0.74). **(1.5 column fitting image, color)**

Isotopic values show a wide range: δ^2H between -26.5‰ and +4.4‰ and $\delta^{18}O$ between -4.6‰ and +0.2, although the majority of groundwater samples is more isotopically depleted, plotting near or slightly above both LMWL and GMWL. Values of δ^2H excess, more commonly known as deuterium (D) excess

(and calculated as $\delta^2H-8*\delta^{18}O$) are high for most groundwater and rainwater samples (up to +19.8‰, mean of +12.8‰) when compared to the GMWL (+10 ‰), whereas a few samples plot below the GMWL line. Groundwater samples seem to plot along a line with slope of 5.4, much lower than the slope of 8.7 of the LMWL. Regarding the spatial distribution, the more enriched samples originate from shallow groundwater from areas of lower recharge around the Incomati valley and in the southwest, whereas the highest D excess values are found in groundwater below the urban areas (Fig. 2).

The main hydrochemical characteristics of the collected samples are exposed for individual WT's below. Ion ratios and concentrations plotted *vs.* Cl^- concentrations, as well as Ca^{2+} *vs.* SO_4^{2-} concentrations, and [Ca+Mg] *vs.* HCO_3^- concentrations are presented in Fig. 5 for assessing the evolution and relation of major ions in the aquifer from fresh to brackish/salt waters. Mixing trajectories presented in the plots were calculated considering a conservative mixing model for freshwater (mean WT-1 composition) and seawater (VSMOW) end-members according to Eq. 1:

$$m_{i,mix} = f_{sea} \cdot m_{i,sea} + m_{i,fresh} \cdot (1 - f_{sea}) \qquad \text{Eq. 1}$$

where m_i is the concentration of ion *i* in mmol/l; f_{sea} represents the fraction of seawater in the mixture; and *mix*, *sea*, and *fresh* subscripts indicate conservative mixture, seawater and freshwater ion concentrations, respectively (Appelo and Postma, 2005). The distribution of samples for both aquifers is further presented in Fig. 6.

WT-1

WT-1 represents the largest group of samples in the area, mainly located in dune areas in both the phreatic and semi-confined aquifers (Fig. 6). These samples represent freshwaters with the lowest EC values (53-545 µS/cm) and Cl^- concentrations (<4 meq/l). Mean Na/Cl ratio is 1.08, ranging from 0.7 to 1.138 (Fig. 5a). The samples present generally low HCO_3^-, Ca^{2+} and SO_4^{2-} concentrations, albeit with high standard deviations.

WT-2

Groundwater samples from WT-2 are mainly located around peri-urban areas of Maputo and Matola cities (Fig. 6). Most samples are classified as shallow freshwater, presenting a small range of EC (636 - 824 µS/cm) and Cl^- concentrations (1 - 4.6 meq/l), bhough values are higher than WT-1. Mean Na/Cl ratio is very high (1.48) with few samples below the ocean ratio and decreasing ratio with increasing Cl^- concentration (Fig. 5a). As in WT-1, the range in HCO_3^- concentrations is large, but overall values are higher, increasing from the coast towards inland and with higher values in the semi-confined aquifer. Mg^{2+} and Ca^{2+} concentrations are higher and with a narrower range than in WT-1 (Fig. 5e). SO_4/Cl ratios are high and Ca/SO_4 ratios range from 0.3 to 2 (average slightly above 1, Fig. 5b and 5d).

WT-3

WT-3 is characterized by the upper range of freshwater, more mineralized than WT-1 and WT-2, with EC 930-1460 µS/cm and Cl^- 2.8-7.5 meq/l. Samples are taken from both the unconfined and semi-confined aquifers and located along the Matola River and near the Maputo city coastline (Fig. 6). Na/Cl ratios are generally above the oceanic ratio (mean value of 1.37 meq/l, Fig 5a). Mg^{2+}, SO_4^{2+} and HCO_3^- concentrations are significantly higher than in WT-1 and WT-2. The SI for calcite is around 0. Furthermore, these samples exhibit a higher correlation between [Ca+Mg] and HCO_3^- in comparison to other water groups (Fig 5e). The Br/Cl ratios show a range from 1E-03 (below the ocean ratio) to 2E-03 (above the oceanic ratio). As in the previous two water type groups, there is a large spread in the δ^2H and $\delta^{18}O$ values.

WT-4

WT-4 represents a group of six brackish/salt water samples, two collected in the unconfined aquifer near the western border in the North and near the Matola River in the South, and four in the semi-confined aquifer, to the West of the Matola River (Fig. 6). With a much higher salinity in comparison with previous water groups, EC ranges between 2600 and 5250 µS/cm and the Cl^- concentration between 18

and 35 meq/l. Na/Cl ratios are usually below the oceanic ratio (mean value of 0.73 meq/l, Fig. 5a). Alkalinity is moderate to high (between 1.1 and 6.1 meq/l). Br/Cl ratios are only slightly below the oceanic ratio. Remarkable are the low SO_4/Cl ratios and high concentrations of Mg^{2+}, and particularly Ca^{2+}, with very high Ca/HCO_3 and Ca/SO_4 ratios, shifting towards a $CaCl_2$ water type. WT-4 has a relatively narrow range in δ^2H and $\delta^{18}O$ values, between -11.3‰ and -20.7‰, and between -4.5‰ and -3.4‰, respectively.

WT-5

WT-5 consists of two surface water samples from the Matola River (Fig. 6). EC and Cl^- concentrations are the highest among samples (respectively 14700-17680 µS/cm and 150-185 meq/l). Samples show moderate to high alkalinity (around 6 meq/l), low Na/Cl ratios (mean value of 0.51) and a Br/Cl ratio of 0.0012, near the oceanic ratio. SO_4/Cl ratios are high compared to the other brackish samples, plotting slightly above the oceanic ratio, Fig. 5b. WT-5 further shows an enriched isotopic composition, ranging from +3.1‰ to +4.4‰ for δ^2H, and from -1.0‰ to +0.2‰ for $\delta^{18}O$.

WT-6

WT-6 is represented by only one water sample, showing singular characteristics, therefore, being in a separate group. EC is 9200 µS/cm and Cl^- concentration equals 59 meq/l. The Na/Cl, SO_4/Cl and Br/Cl ratios are near oceanic values, while Mg^{2+} concentrations are rather high. The sample was collected from the semi-confined aquifer near Matola River on the southwest of study area (Fig. 6).

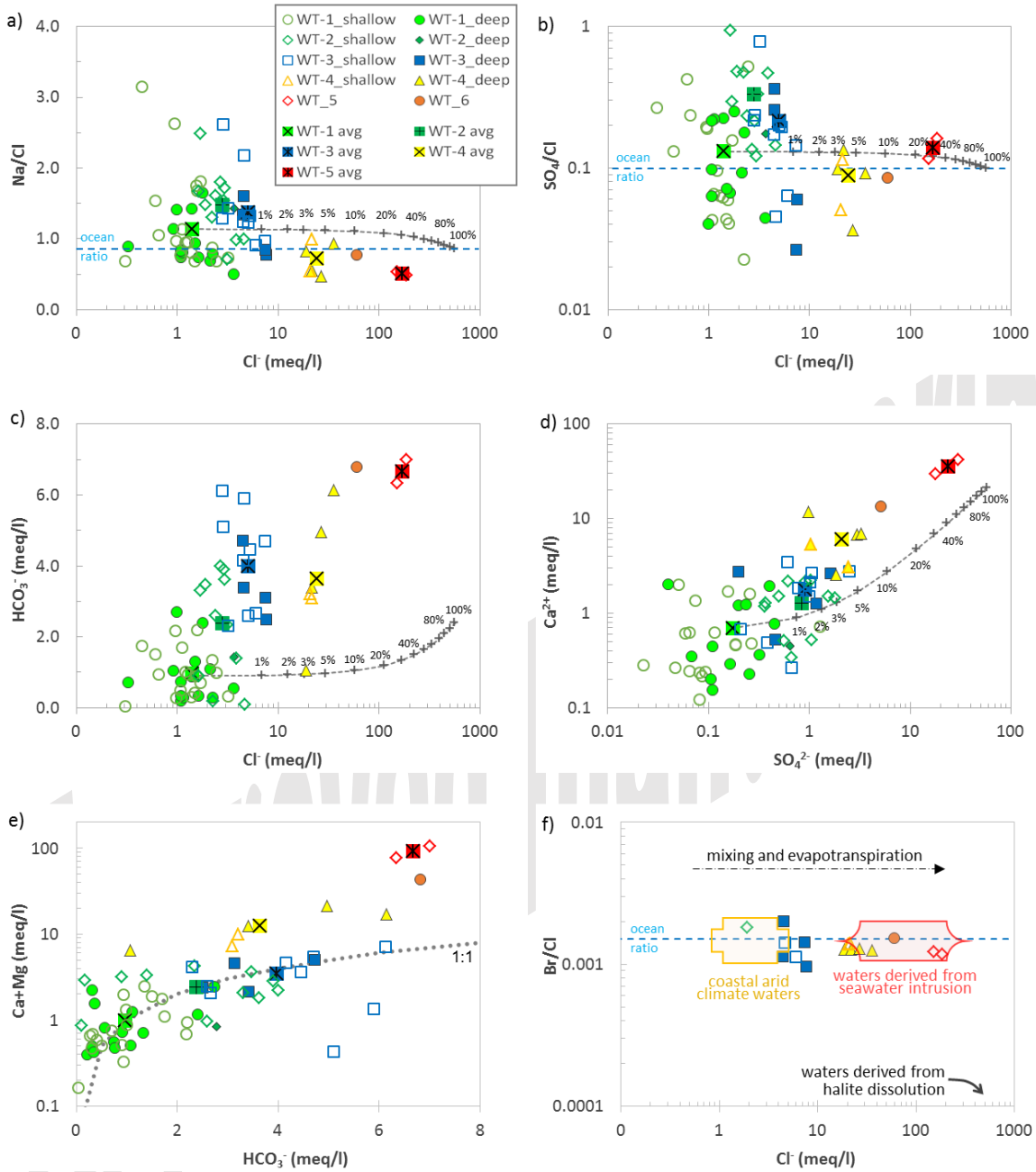

Fig. 5: Hydrochemical relationships between selected ions in meq/l. Water samples labelled according to WT groups, with mean composition of WTs presented in different symbols. Open symbols represent shallow groundwater (and surface water) samples, while filled symbols represent deep groundwater samples. Conservative mixing lines showed with % of seawater contribution to final solution. Ocean ratios are showed in dashed blue lines. Red circles in Fig. 5e highlight samples with a surplus of [Ca+Mg] compared to HCO_3^-, while blue circle demarks

samples with a surplus of HCO_3^-. Reference values in Fig. 5f according to Alcala and Custodio (2008) and Han et al. (2013). **(2 columns fitting image, color)**

The spatial distribution of water samples for both phreatic and semi-confined aquifers is presented in Fig. 6 together with interpolated EC contours. Other than the abundant presence of freshwaters in both aquifers under the recent and old dune areas, hydrochemical water types do not show a very strong zonation in the area. Notwithstanding, all but one brackish/salt water samples are located in the west and in the semi-confined aquifer, to the west of the Matola River (which itself is also saline, WT-5), forming a near to parallel line to the actual coast line. Samples of WT-3 occur in the transition between the fresh and brackish water types, both in vertical direction (wells in unconfined aquifer, e.g. SGW 4, 9, 11, 37, 51, 61 and horizontal direction (e.g. DGW17 and DGW38). Samples collected from downstream areas of the Incomati River are fresh, but high EC was measured in small tributaries in the North (4500 µS/cm, Fig. 1).

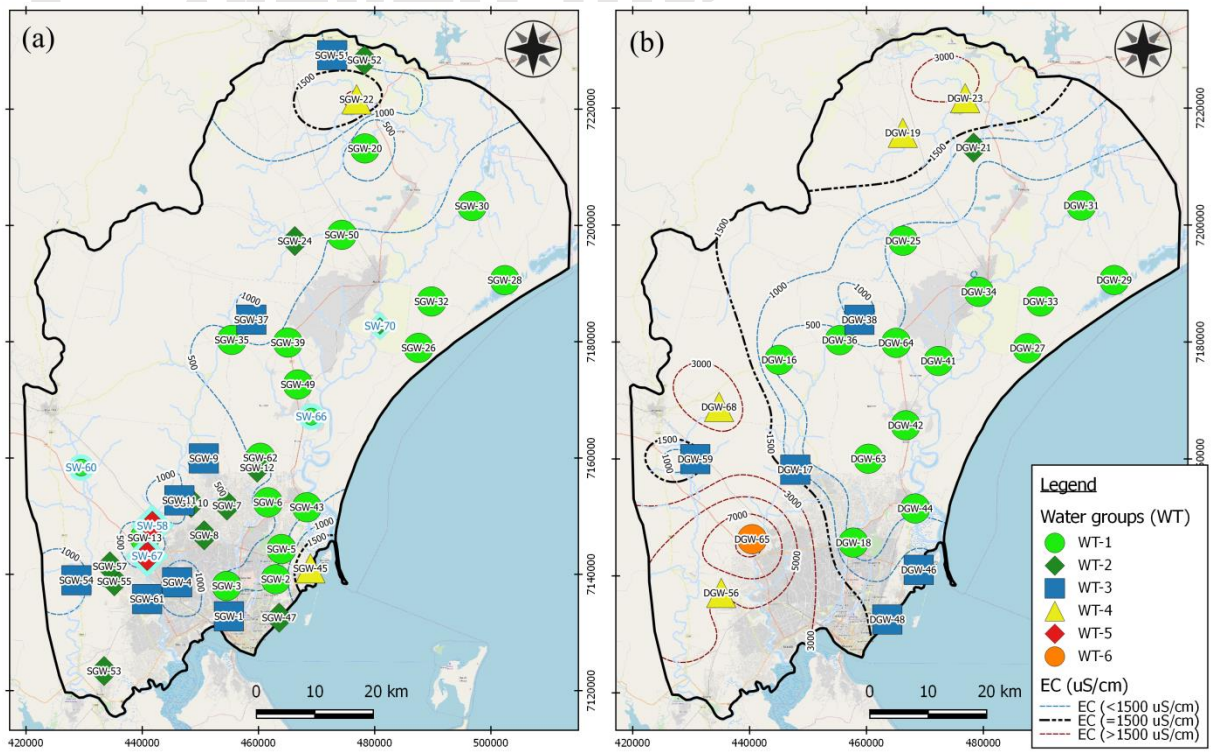

Fig. 6: Distribution of water types in the (a) phreatic, and (b) semi-confined aquifers together with contours of field EC measurements (µS/cm). Surface water samples are presented with blue labels together with samples from the phreatic aquifer. **(2 columns fitting image, color)**

5. Discussion

5.1 Origin of groundwater

Two main hypotheses can be provided for the origin of groundwater isotopically depleted in $\delta^{18}O$ and $\delta^{2}H$, as is observed in most WT groups and at both shallow and deep levels, with the exception of WT-5, a few samples from open hand-dug wells and from areas near the coastline and of the Incomati valley (Fig. 2):

1) Groundwater is predominantly derived from recharge during heavy storm events, which are often isotopically depleted. Recent work from Andreetta (2018) has found recharge rates in the area to be largely affected by rainfall intensity (particularly significant above 25 mm/day), runoff threshold and canopy interception. These results are in agreement with Taylor et al. (2012), who show that extreme daily precipitation events can be critical for groundwater recharge in semi-arid regions, and is equally observed by Thomas et al. (2016).

2) Groundwater has a strong component of recharge from land-derived re-evaporated rainwater that is isotopically depleted, with a stronger depletion in ^{18}O and with high deuterium (D) excess values (Adelana et al., 2015; Appelo and Postma, 2005; Mook, 2001). Even though one might not expect a significant re-evaporated rainwater component near the coast, strong evaporation from rainwater can be promoted by dense canopies and consequently strong interception, found to be very relevant in the study area (Andreetta, 2018). The hypothesis is reinforced by the low slope of the groundwater sample regression line (5.4), significantly lower than that of the LMWL (8.7). In fact, evaporation itself becomes particularly evident for a number of samples from freshwater type groups WT-1, WT-2 and WT-3 near

the coast and in the Incomati valley, and for the Matola brackish/salt water samples (WT-5), all of which are more enriched in the heavier isotopes (for example, groundwater samples SGW26, DPW27, SGW30, SGW47, DGW48 located in areas classified with limited recharge potential, Fig. 2). This is further revealed by looking at the conservative mixing model in the scatter plot of $\delta^{18}O$ *vs*. Cl^- (Fig.7). In the plot, several freshwater samples plot well above the conservative mixing line, showing a stronger enrichment of $\delta^{18}O$ than Cl^- concentration increase. As opposed to transpiration, which does not cause fractionation, this further indicates the important role of direct evaporation from land and vegetation canopy (i.e. interception) as a concentration mechanism of recharge water (e.g., Currell et al, 2015; Han et al., 2013; Mongelli et al., 2013). The deviation from the conservative mixing line is further particularly large for the samples from WT-5, suggesting the wetland experiences strong evaporation of groundwater seepage.

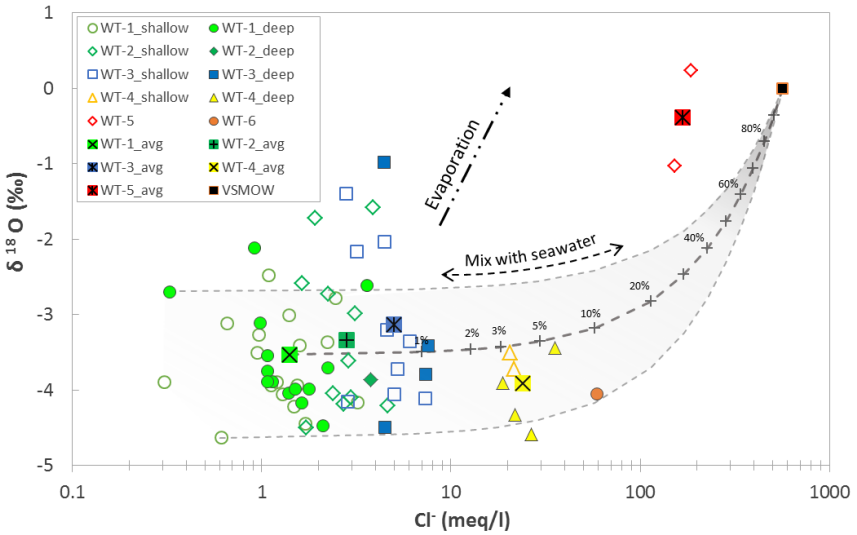

Fig. 7: $\delta^{18}O$ *vs.* Cl^- plot along with conservative mixing line between freshwater and seawater (VSMOW) end-members. Mixing trajectory and proportions were calculated through conservative mixing mass balance equation (Eq. 1). Theoretical trajectories of mixing and evaporation processes are presented in thicker dashed arrows. **(1.5 column fitting image, color)**

5.2 Salinization and freshening

For the brackish/saltwater groups WT-4, WT-5 and WT-6 the Br/Cl ratio was used in combination with major ion and stable isotope analysis to assess the source of salinity. Br^- behaves conservatively during evaporation processes, being concentrated in the brine. Its ratio with Cl^- remains equal until halite saturation, after which Br^- starts to be incorporated in small amounts within halite crystals (Cendón et al., 2004; McCaffrey et al., 1987). Therefore, residual brines and waters originating from mixing with paleo-seawater present Br/Cl ratios above or near the ocean value of $1.5x10^{-3}$. In contrast, groundwater dissolving evaporites shows a much lower ratio, around $1.0x10^{-4}$ (Alcala and Custodio, 2008; Edmunds, 1996; Han et al., 2015; Liu et al., 2015; Mollema et al., 2013; Siemann and Schramm, 2000).

Water samples of the study area present Br/Cl ratios ranging from $9.7x10^{-4}$ to $2.0x10^{-3}$ (Fig. 5f). No significant differences are observed in Br/Cl ratios among brackish/saline surface water and shallow and deep groundwater. Freshwater samples plot around the ocean ratio and within the domain of coastal arid climate waters, indicating strong influence from sea moisture as expected for coastal freshwaters (Alcala and Custodio, 2008). Brackish/saltwater samples plot close and slightly below the ocean ratio, within the seawater intrusion domain, suggesting their origin is related to mixing with seawater and/or evapotranspiration, rather than halite dissolution. Among the former two, the $\delta^{18}O$ *vs.* Cl^- plot strongly supports mixing with seawater for all brackish water groups, and additional evaporation for WT-5 (Fig. 7). However, all but one of these samples are located far inland, predominantly in the semi-confined aquifer, with a hydraulic head tens of meters above sea level (Fig. 6). From this information it is inferred that the local salinity source must be derived from mixing with old seawater that intruded into the subsurface in periods of high sea level, and that is currently trapped in the aquitards. As described in the literature, the Mozambican coast experienced numerous transgressions and regressions between the Cretaceous and the Quaternary, with some of the paleo-coastlines located more than 50 km inland from the actual shoreline (Förster, 1975; Salman and Abdula, 1995). The same authors discuss the absence of evaporites near the Great Maputo area, although they are observed in the north of the province,

corroborating our findings. Lee et al. (2016), Narany et al. (2014) and Vengosh et al. (1999), among others, also discuss how trapped seawater was distinguished from other processes to constitute an important salinization mechanism in coastal semi-arid regions.

The co-existence of high Cl^- and HCO_3^- concentrations in WT-4, WT-5 and WT-6 (Fig. 5c) provides an indication of mixing between fresh and saline water having occurred prior to, or together with, mineral dissolution in a CO_2-rich environment. This could either indicate vertical saltwater intrusion in times of high sea level and linked to storm surges, or reveal mixing with freshwater rich in CO_2 but with low alkalinity, followed by mineral dissolution. The latter seems quite possible as the unconfined aquifer is poor in carbonate minerals, so that recharge water can infiltrate and maintain a high dissolved CO_2 content. Mixing with old seawater then either occurs in the carbonate-richer semi-confined aquifer together with (closed system) calcite dissolution, or in the silicate mineral unconfined aquifer (and aquitard) with sufficient time for silicate weathering to take place (depending on the reactivity of the minerals) (Kenoyer and Bowser, 1992).

If on the one hand Cl^- concentrations of WT-4, WT-5 and WT-6 below that of seawater most likely result from mixing/dilution with infiltrating freshwaters (e.g., Mollema et al., 2013), on the other hand the maximum Cl^- concentrations observed in WT-5 are related to evaporation, which does not affect Br/Cl ratios but results in high $\delta^{18}O$ values, as seen in Fig. 7 and successfully modelled in PHREEQC. Hydrochemical modelling in combination with the observation of $CaCl_2$ water subtypes, low Na/Cl ratios (< 0.7) and high Ca/HCO_3 ratios (ranging from 1-6) also revealed the process of cation exchange in the brackish/salt water groups. Upon salinization, Ca^{2+} on the exchanger complex is replaced by Na^{2+} (or Mg^{2+}) from the intruding seawater, as expressed by Eq. 2 (Appelo and Postma, 2005):

$$2Na^+ + Ca\text{-}X \leftrightarrow 2Na\text{-}X + Ca^{2+} \qquad \text{Eq. 2}$$

where X represents the complex exchanger (aquifer material).

The reverse reaction (freshening) can occur in Eq. 2 (from right to left) when freshwater flows into a saltwater aquifer and Na^+ from the complex is replaced by Ca^{2+}, leading to a $NaHCO_3$ water types (Appelo and Postma, 2005). Freshening can be observed in WT-3 and WT-2 water samples located in the area directly east of the Matola River. This process results in secondary calcite dissolution, increasing alkalinity and Na/Cl ratios, while strongly decreasing Ca/HCO_3 ratios, as observed in samples from the referred sector of the area (Fig. 5e). In other words, there seem to be two distinct neighbouring zones in the south separated by the Matola River, west of the river showing salinization and east of the river revealing flushing. A similar but less widespread occurrence of such neighbouring zones is found in the north near a tributary of the Incomati River (Fig. 6).

Mean water compositions of groups WT-4 and WT-5 could also be adequately simulated in PHREEQC through mixing with seawater and cation exchange. Following simulations, both the conservative ion Cl^- and non-conservative ions such as Ca^{2+}, Na^+ and Mg^{2+}, as well as the Br/Cl ratio were near the observed values (Table S.4, supplementary material), with seawater contributions to WT-4 and WT-5 compositions between 4% and 5%.

5.3 Other relevant hydrochemical processes

Rock weathering/dissolution increases groundwater mineralization, mainly reflected in the increase in HCO_3^- concentrations together with major cations. This is either due to presence of highly soluble carbonate minerals (e.g. calcite, dolomite), or due to the slower weathering of silicate minerals such as Ca-bearing plagioclase. In the latter case alkalinity can be an indicator of travel time in younger groundwater (Kenoyer and Bowser, 1992). Conceptually, the most evolved groundwater is expected at larger depths and in the discharge area of the aquifer near the coast, related to deeper and more regional groundwater flow lines. Interestingly this is where WT-1 dominates, with very low alkalinity and EC, revealing that it is predominantly young water derived from local recharge (with very little interaction with the aquifer material - silicate mineral bearing sands), even at larger depths. Indeed it appears that the

aquifer system can be interpreted as a single (unconfined) unit here, since samples show similar isotopic and hydrochemical characteristics. This hypothesis is further supported by borehole descriptions and by the small hydraulic head differences between shallow and deep wells.

EC and alkalinity increase consistently from WT-1 through WT-2 towards WT-3, the latter two located in the centre and in the south of the study area. Many samples are defined as $CaHCO_3$ water subtypes and show a good fit around the 1:1 line on the plot [Ca+Mg] *vs.* HCO_3 (Fig. 5e), indicating that Ca-bearing plagioclase dissolution in the phreatic aquifer and calcite/dolomite dissolution in the semi-confined aquifer are most likely responsible for controlling local hydrochemistry. Samples of WT-2 and WT-3 that plot below the 1:1 line are most likely affected by: 1) Na-silicate weathering, and/or 2) cation exchange linked to freshening of aquifer sectors previously presenting saltwater. Both processes can be similarly inferred from the high Na/Cl ratios (≥ 1.0) observed in many samples (Fig. 5a).

The high correlation observed between Ca^{2+} and SO_4^{2+} (Fig. 5d) could also suggest some gypsum dissolution in the system. However, for brackish/salt waters (WT-4, WT-5 and WT-6) this correlation seems indirect, as SO_4/Cl ratios are rather close to the oceanic ratio (Fig. 5b), and the surplus of Ca^{2+} (with regard to both SO_4^{2-} and HCO_3^-) in these samples is most probably linked to cation exchange. Minor gypsum dissolution could explain the high SO_4/Cl ratios in freshwaters (WT-1, WT-2 and WT-3), although high SO_4^{2-} concentrations from samples below the urban area are more likely related to contamination from domestic and industrial activities (Zghibi et al., 2013). On the contrary, very low SO_4^{2-} concentrations found in WT-1, with SO_4/Cl ratios below the oceanic ratio are related to sulphate reduction (e.g., Andrade and Stigter, 2011), which is supported by the higher CO_2 pressures in these samples (Table S.3, supplementary material).

5.4 Hydrochemical evolution of groundwater

Local available geophysical and borehole information from previous surveys was combined with the current hydrochemical results for a more accurate discussion of salinity origin and its relationship with the hydrogeological context of the area. The cross-section of Fig. 8 was chosen for its representativeness, comprising most water groups and surface water samples from Matola River. Geological delineation was based on available borehole descriptions and previous geophysical surveys – Vertical Electric Sounding (VES) from technical reports (HYDROCONSEIL/WE-Consult, 2011). Differences in groundwater level displayed on the map were interpolated from measurements during the field campaign (Table S.5, supplementary material).

The VES measurements from PZ-14 and PZ-17 reveal low resistivity for the bottom part of the phreatic aquifer and for the aquitard units (~ 15 *Ohm.m* and between 4 – 8 *Ohm.m*, respectively). Following Archie's law ($\Omega = F\ x\ \Omega_{water}$, (Archie, 1942)) and assigning a formation factor of 2-3 for the aquitard unit (silty marl and clay), porewater EC can be calculated as 3000 – 8000 µS/cm), revealing up to 10% mixing with seawater. This indication, together with the Br/Cl ratios and hydrochemical models suggest that the aquitard unit in the area still contains trapped seawater, probably already diluted in some locations. These findings support mixing as being one of main local salinization mechanisms and summarized as follows: trapped saltwater flows up or down from the aquitard unit led by local head differences, mixes with freshwater, and results in observed brackish/salt waters. Mixing triggers cation exchange and, as previously expressed, results in $CaCl_2$ water subtypes as observed in WT-4 samples.

Furthermore, around the Matola River it can be observed that hydraulic heads of the semi-confined aquifer are (slightly) higher than those of the phreatic aquifer, resulting in an upward flow (Fig. 8). This can explain the occurrence of brackish/salt waters in the river since trapped saltwater is brought to shallower levels of the aquifer, subsequently discharging into the river. Upon seepage and consecutive evaporation, both salinity and $\delta^{18}O$ increase, as stressed in previous sections. This dynamic salinization

mechanism is most likely seasonally controlled and linked to recharge rates and hydraulic head fluctuations, since the river may act as a natural hydraulic gradient driver on the system, allowing a greater upward flux of saltwater during dry seasons and low river flow. So that, the pictured hydraulic heads distribution can be somewhat different during rainy seasons, resulting in different flow patterns. Also, surface seawater incursion and its subsequent streambed entrapment cannot be disregarded as a potential salinization mechanism in the river, especially when considering sea level rise. The brackish/salt water sample from PZ02 (far right on cross section, Fig. 8) is most likely linked to mixing with modern seawater. While corresponding to group WT-4, the sample is located near the coast at shallow depth, plots somewhat closer to the mixing line in the plot $\delta^{18}O$ *vs.* Cl^- and shows a slightly enriched isotopic signature that resembles modern intruded seawater mixing with freshwater.

Slightly higher salinities in brackish/salt waters samples in the north in comparison to samples in the south can be linked to different recharge patterns in the area. Computed recharge potentials and rates indicate that higher rates in the south can lead to a faster dilution of salt waters, while low infiltration rates and high ETP values in the north result in smaller dilution rates and a prevalence of more saline waters. The previous existence of saltwater in areas with high recharge potential and rates, such as the dune belts near the coast, cannot be excluded, as saltwater will have been flushed out to a larger extent by freshwater inflow. Sampling at a higher spatial resolution and combining it with numerical modelling could help further detail the spatial distribution and expected temporal evolution of saltwater occurrence, supporting water management in the area.

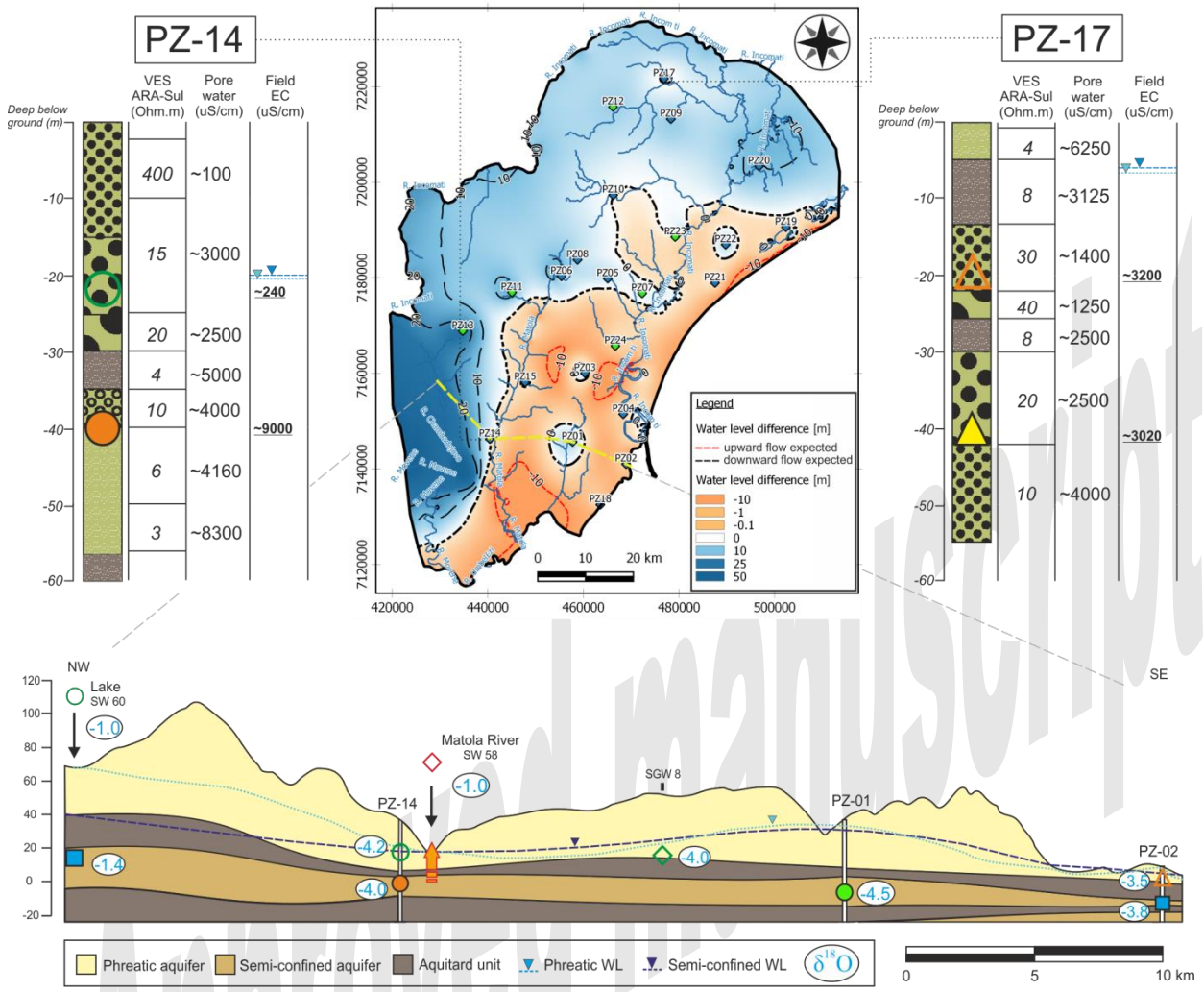

Fig. 8: (*top*) Map of water level (WL) differences derived from field measurements (April, 2017) (blue areas = downward flow expected; orange areas = upward flow expected); borelogs of PZ14 and PZ17 are shown together with previous VES/EC measurements, collected groundwater samples labelled according to defined WT groups and field EC and water level measurements in the wells (April, 2017); porewater resistivity values were calculated through Archie's law; (*bottom*) cross section view of the area with water samples and respective $\delta^{18}O$ values; orange arrow in the cross section indicates location of possible groundwater upward flow; the location of the cross section is represented by the dashed yellow line on the map; mind the vertical exaggeration of the profile. **(2 columns fitting image, color)**

6. Conclusions

The present study provides a detailed assessment of the possible origins of freshwater and saltwater in surface and groundwater of the semi-arid region of Great Maputo, by employing a combination of multivariate statistical, hydrochemical, isotopic, geophysical and recharge assessment tools. Six different water groups have been classified using HCA, from fresh to brackish/salt waters. Mixing with relic saltwater as main salinization mechanism is simultaneously supported by location, piezometry, physico-chemical parameters, a conservative mixing model (Cl^- and $\delta^{18}O$) and the Br^- signature of brackish/salt waters. Geophysical and piezometer data suggest that the local aquitard unit is a main source of inland saltwater in the area, which contains relic saltwater probably trapped during the last transgression period and remaining as lenses within the unit due to its low permeability. Trapped saltwater migrates up or down from the unit according to local hydraulic gradients, resulting in observed brackish/salt groundwater. Following seepage into surface water, evapoconcentration further increases salinity and $\delta^{18}O$ values of the rivers in the western sector (Matola) and northern sector (tributary of Incomati). Mixing with surface water from upstream and drainage from the sand dunes gives the Incomati River mostly a freshwater signature. Fresh groundwater originates from rainfall and evapotranspiration, with higher direct evaporation rates observed in the stable isotope signature in the lower recharge areas; it is further influenced by rock weathering, with silicate minerals dominating in the phreatic aquifer and more carbonate rich material in the semi-confined aquifer.

The present results are of great relevance for water management in the area, elucidating crucial points concerning the aquifer system and its potential for exploitation, within a context of salinization but also freshening in important recharge areas. The research emphasizes the successful application of complementary set of tools and approaches for assessing hydrochemistry and distinguishing salinity origins in semi-arid coastal areas. The available chemical and isotope data presented do not allow determination of groundwater ages for an enhanced understanding of entrapment or mixing processes, and groundwater travel times. The use of numerical models and a more comprehensive isotopic study

involving radioactive isotopes such as ^{14}C and ^{3}H should be considered for an accurate assessment of sea level changes and periods of transgression and subsequent saltwater entrapment. A comparison of $^{36}Cl/Cl$ in the phreatic and semi-confined aquifers, as well as at selected locations along the Matola River and coastline would be also interesting for confirming and distinguishing different sources of salinity in what concerns age and source. The methodology here presented can be transferred to other sites and may provide a reliable base for the development of effective mitigation and adaptation strategies for saltwater occurrence.

Acknowledgments

This study was financially supported by the Dutch Ministry of Foreign Affairs (DUPC) under the SALINPROVE Project led by IHE Delft, and the Erasmus+ Mundus Joint Master Programme in Groundwater and Global Change – Impacts and Adaptation (GroundwatCh). Assistance during field work by ARA-SUL and UEM staff is gratefully acknowledged. The authors also would like to thank Philippa Higgins, Dioni Cendón and a third anonymous reviewer for detailed comments on previous versions of this manuscript.

References

Adelana, S.M., Allinson, G., Kitching, M., Ii, H., Salzman, S., Mcnamara, E., Taniguchi, M., Croatto, G., Shelley, B., 2015. Flow, Recharge and Mixing Processes in the Werribee Basin (Australia) Using Natural Environmental Isotope Geochemistry: Implications for Water Resources Management.

Adonis, S., 2007. The Hydrochemical Characteristics of Groundwater in the Incomati Estuary. Western Cape.

Alcala, F.J., Custodio, E., 2008. Using the Cl / Br ratio as a tracer to identify the origin of salinity in aquifers in Spain and Portugal. J. Hydrol. 189–207. https://doi.org/10.1016/j.jhydrol.2008.06.028

Andrade, A.I.A.S.S., Stigter, T.Y., 2011. Hydrogeochemical controls on shallow alluvial groundwater under agricultural land: Case study in central Portugal. Environ. Earth Sci. 63, 809–825. https://doi.org/10.1007/s12665-010-0752-7

Andrade, A.I.A.S.S., Stigter, T.Y., 2009. Multi-method assessment of nitrate and pesticide contamination in shallow alluvial groundwater as a function of hydrogeological setting and land use. Agric. Water Manag. 96, 1751–1765. https://doi.org/10.1016/j.agwat.2009.07.014

Andreetta, R., 2018. Impact of climate change on groundwater recharge in the Great Maputo Aquifer, Mozambique. UNESCO-IHE, Delft.

Appelo, C.A.J., Postma, D., 2005. Geochemistry, Groundwater and Pollution - 2nd Edition. Amsterdam.

Archie, G.E., 1942. The Electrical Resistivity Log as an Aid in Determining Some Reservoir Characteristics. Pet. Trans. AIME 146, 54–62. https://doi.org/https://doi.org/10.2118/942054-G

Barlow, P.M., Reichard, E.G., 2010. L'intrusion d'eau salée dans les régions côtières d'Amérique du Nord. Hydrogeol. J. 18, 247–260.

https://doi.org/10.1007/s10040-009-0514-3

Bonilla Valverde, J., Blank, C., Roidt, M., Schneider, L., Stefan, C., 2016. Application of a GIS Multi-Criteria Decision Analysis for the Identification of Intrinsic Suitable Sites in Costa Rica for the Application of Managed Aquifer Recharge (MAR) through Spreading Methods. Water 8, 391. https://doi.org/10.3390/w8090391

Bouchaou, L., Michelot, J.L., Vengosh, A., Hsissou, Y., Qurtobi, M., Gaye, C.B., Bullen, T.D., Zuppi, G.M., 2008. Application of multiple isotopic and geochemical tracers for investigation of recharge , salinization , and residence time of water in the Souss – Massa aquifer , southwest of Morocco 267–287. https://doi.org/10.1016/j.jhydrol.2008.01.022

BURGEAP, 1962. Hydrogeologie du Sud du Save.

Cendón, D.I., Peryt, T.M., Ayora, C., Pueyo, J.J., Taberner, C., 2004. The importance of recycling processes in the Middle Miocene Badenian evaporite basin (Carpathian foredeep): Palaeoenvironmental implications. Palaeogeogr. Palaeoclimatol. Palaeoecol. 212, 141–158. https://doi.org/10.1016/j.palaeo.2004.05.021

Chairuca, L., Naafs, A., van Haren, I., Upton, K., Ó Dochartaigh, B.É., 2016. Hydrogeology of Mozambique. Earthwise.

Chi, G., Savard, M.M., 1997. Sources of basinal and Mississippi Valley-type mineralizing brines: mixing of evaporated seawater and halite-dissolution brine. Chem. Geol. 143, 121–125. https://doi.org/10.1016/S0009-2541(97)00096-X

Craig, H., 1961. Isotopic variation in meteoric waters. Science (80-.). 133, 1702–1703.

Currell, M.J., Cartwright, I., Bradley, D.C., Han, D., 2010. Recharge history and controls on groundwater quality in the Yuncheng Basin, north China. J. Hydrol. 385, 216–229. https://doi.org/10.1016/j.jhydrol.2010.02.022

Currell, M.J., Dahlhaus, P., Ii, H., 2015. Stable isotopes as indicators of water and salinity sources in a southeast Australian coastal wetland: identifying relict marine water, and implications for future change. Hydrogeol. J. 23, 235–248. https://doi.org/10.1007/s10040-014-1199-9

de Louw, P.G.B., Oude Essink, G.H.P., Stuyfzand, P.J., van der Zee, S.E.A.T.M., 2010. Upward groundwater flow in boils as the dominant mechanism of salinization in deep polders, The Netherlands. J. Hydrol. 394, 494–506. https://doi.org/10.1016/j.jhydrol.2010.10.009

DNA, 1988. Groundwater Management in Grande Maputo. Maputo.

Douglas S. Cherkauer, 2003. Quantifying Groundwater Recharge at Multiple Scales Using PRMS and GIS. Groundwater 42, 97–110.

Edmunds, W.M., 1996. Bromine geochemistry of British groundwaters 60, 275–284.

Edmunds, W.M., Ma, J., Aeschbach-Hertig, W., Kipfer, R., Darbyshire, D.P.F., 2006. Groundwater recharge history and hydrogeochemical evolution in the Minqin Basin, North West China. Appl. Geochemistry 21, 2148–2170. https://doi.org/10.1016/j.apgeochem.2006.07.016

El Yaouti, F., El Mandour, A., Khattach, D., Benavente, J., Kaufmann, O., 2009. Salinization processes in the unconfined aquifer of Bou-Areg (NE Morocco): A geostatistical, geochemical, and tomographic study. Appl. Geochemistry 24, 16–31. https://doi.org/10.1016/j.apgeochem.2008.10.005

FAO, F. and A.O. of the U.N., 2015. FAO GEONETWORK.

Ferguson, G., Gleeson, T., 2012. Vulnerability of coastal aquifers to groundwater use and climate change. Nat. Clim. Chang. 2, 342–345. https://doi.org/10.1038/NCLIMATE1413

FIPAG, FICHTNER, AUSTRALCOWI, 2012. Estudos Ambientais e Sociais para o Sistema de Abastecimento de Água do Grande Maputo. Maputo.

Förster, R., 1975. The Geological History of the Sedimentary Basin of Southern Mozambique, and some Aspects of the Origin of the Mozambique Channel. Palaeogeogr., Palaeoclim. Palaeoecol., 17, 267–287.

Ghesquière, O., Walter, J., Chesnaux, R., Rouleau, A., 2015. Scenarios of groundwater chemical evolution in a region of the Canadian Shield based on multivariate statistical analysis. J. Hydrol. Reg. Stud. 4, 246–266. https://doi.org/10.1016/j.ejrh.2015.06.004

Giménez, E., Bencini, A., Pranzini, G., 2010. Hydrogeochemical considerations about the origin of groundwater salinization in some coastal plains of Elba Island (Tuscany, Italy). Environ. Geochem. Health 32, 243–257. https://doi.org/10.1007/s10653-009-9281-2

Giménez, E., Morell, I., 1997. Hydrogeochemical analysis of salinization processes in the coastal Aquifer of Oropesa (Castellon, Spain). Environ. Geol. 29, 118–131. https://doi.org/10.1007/s002540050110

Güler, C., Thyne, G., 2004. Hydrologic and geologic factors controlling surface and groundwater chemistry in Indian Wells-Owens Valley area , southeastern California , USA 285, 177–198. https://doi.org/10.1016/j.jhydrol.2003.08.019

Haberle, J., Svoboda, P., 2015. Calculation of available water supply in crop root zone and the water balance of crops. Contrib. to Geophys. Geod. 454, 285–298. https://doi.org/10.1515/congeo-2015-0025

Han, D., Kohfahl, C., Song, X., Xiao, G., Yang, J., 2011. Geochemical and isotopic evidence for palaeo-seawater intrusion into the south coast aquifer of Laizhou Bay, China. Appl. Geochemistry 26, 863–883. https://doi.org/10.1016/j.apgeochem.2011.02.007

Han, D., Post, V.E.A., Song, X., 2015. Groundwater salinization processes and reversibility of seawater intrusion in coastal carbonate aquifers. J. Hydrol. 531, 1067–1080. https://doi.org/10.1016/j.jhydrol.2015.11.013

Han, D., Song, X.F., Currell, M.J., Yang, J.L., Xiao, G.Q., 2013. Chemical and isotopic constraints on evolution of groundwater salinization in the coastal plain aquifer of Laizhou Bay, China. J. Hydrol. 508, 12–27. https://doi.org/10.1016/j.jhydrol.2013.10.040

Healy, R.W., 2010. Estimating Groundwater Recharge. Cambridge University Press.

Heston, D., 2015. Using Chloride and Bromide Mass Ratios and Binary Mixing Curves to Evaluate Anthropogenic Influences on Groundwater in Lycoming and Wayne counties , Pennsylvania.

Hiscock, K.M., Bense, V.F., 2014. Hydrogeology: principles and Practice, 2nd editio. ed. Wiley Blackwell.

HYDROCONSEIL/WE-Consult, 2011. Monitoring MMA Aquifer – Quantative and Qualitative Aspects. Maputo.

Iverach, C.P., Cendón, D.I., Meredith, K.T., Wilcken, K.M., Hankin, S.I., Andersen, M.S., Kelly, B.F.J., 2017. A multi-tracer approach to constraining artesian groundwater discharge into an alluvial aquifer. Hydrol. Earth Syst. Sci. 21, 5953–5969. https://doi.org/10.5194/hess-21-5953-2017

IWACO, 1986. Study of Groundwater to Supply Maputo – Summary of the Hydrogeology of the Study Area. Maputo.

Juizo, D., 1995. Modelação Geohidrológica do Sistema Aquifero da Zona Norte de Maputo.

Kenoyer, G., Bowser, C., 1992. Groundwater chemical evolution in a sandy silicate aquifer in northern Wisconsin: 1. Patterns and rates of change. Water Resour. Res. 28, 579–589.

Kottek, M., Grieser, J., Beck, C., Rudolf, B., Rubel, F., 2006. World map of the Köppen-Geiger climate classification updated. Meteorol. Zeitschrift 15, 259–263. https://doi.org/10.1127/0941-2948/2006/0130

Kovács, J., Erőss, A., 2017. Statistically optimal grouping using combined cluster and discriminant analysis (CCDA) on a geochemical database of thermal karst waters in Budapest. Appl. Geochemistry 84, 76–86. https://doi.org/10.1016/j.apgeochem.2017.05.009

Krause, E.F., 1987. Taxicab Geometry. Dover.

Lee, S., Currell, M., Cendón, D.I., 2016. Marine water from mid-Holocene sea level highstand trapped in a coastal aquifer: Evidence from groundwater isotopes, and environmental significance. Sci. Total Environ. 544, 995–1007. https://doi.org/10.1016/j.scitotenv.2015.12.014

Liu, F., Song, X., Yang, L., Zhang, Y., Han, D., Ma, Y., Bu, H., 2015. Identifying the origin and geochemical evolution of groundwater using hydrochemistry and stable isotopes in the Subei Lake basin , Ordos energy base , Northwestern China. Hydrol. Earth Syst. Sci. 19, 551–565. https://doi.org/10.5194/hess-19-551-2015

Magesh, N.S., Chandrasekar, N., Soundranayagam, J.P., 2012. Delineation of groundwater potential zones in Theni district, Tamil Nadu, using remote sensing, GIS and MIF techniques. Geosci. Front. 3, 189–196. https://doi.org/10.1016/j.gsf.2011.10.007

Marconi, V., Antonellini, M., Balugani, E., Dinelli, E., 2011. Hydrogeochemical characterization of small coastal wetlands and forests in the Southern Po plain (Northern Italy). Ecohydrology 4, 597–607. https://doi.org/10.1002/eco.204

Martinez, J.L., Raiber, M., Cendón, D.I., 2017. Using 3D geological modelling and geochemical mixing models to characterise alluvial aquifer recharge sources in the upper Condamine River catchment, Queensland, Australia. Sci. Total Environ. 574, 1–18. https://doi.org/10.1016/j.scitotenv.2016.09.029

Matsinhe, N.P., Juízo, D., Rietveld, L.C., Persson, K.M., 2008. Water services with independent providers in peri-urban Maputo: Challenges and opportunities for long-term development. Water SA 34, 411–420.

McCaffrey, M.A., Lazar, B., Holland, H.D., 1987. The Evaporation Path of Seawater and the Coprecipitation of Br- and K+ with Halite. SEPM J. Sediment. Res. Vol. 57. https://doi.org/10.1306/212F8CAB-2B24-11D7-8648000102C1865D

Mollema, P.N., Antonellini, M., Dinelli, E., Gabbianelli, G., Greggio, N., Stuyfzand, P.J., 2013. Hydrochemical and physical processes influencing salinization and freshening in Mediterranean low-lying coastal environments. Appl. Geochemistry 34, 207–221. https://doi.org/10.1016/j.apgeochem.2013.03.017

Mongelli, G., Monni, S., Oggiano, G., Paternoster, M., Sinisi, R., 2013. Tracing groundwater salinization processes in coastal aquifers: a hydrogeochemical and isotopic approach in the Na-Cl brackish waters of northwestern Sardinia, Italy. Hydrol. Earth Syst. Sci. 17, 2917–2928. https://doi.org/10.5194/hess-17-2917-2013

Mook, W.G., 2001. Environmental Isotopes in the Hydrological Cycle Principles and Applications Environmental Isotopes in the Hydrological Cycle Principles and Applications, Introducti. ed. UNESCO – IAEA, Paris, Vienna.

Muiuane, E., 2007. The Quality of Groundwater in and around Maputo city, Mozambique, Department of Geology, Eduardo Mondlane University. Maputo.

Narany, T.S., Ramli, M.F., Aris, A.Z., Nor, W., Sulaiman, A., Juahir, H., Fakharian, K., 2014. Identification of the Hydrogeochemical Processes in Groundwater Using Classic Integrated Geochemical Methods and Geostatistical Techniques , in Amol-Babol Plain , Iran. Sci. World J. 2014. https://doi.org/10.1155/2014/419058

Nogueira, G.E.H., 2017. Tracing the Hydrochemical Water Types and Salinization Mechanisms in the Great Maputo Area as a Function of Groundwater Recharge, Hydrogeological Properties and Human Activities. IHE-Delft.

Post, V.E.A., 2005. Fresh and saline groundwater interaction in coastal aquifers: Is our technology ready for the problems ahead? Hydrogeol. J. 13, 120–123. https://doi.org/10.1007/s10040-004-0417-2

Rosário Dias, L.A.X., 2016. IMPACTO DA PROLIFERAÇÃO DE FUROS NA REGIÃO DO MAPUTO. Universidade Eduardo Mondlane.

Rozanski, K., Fröhlich, K., Mook, W., 2001. Environmental Isotopes in the Hydrological Cycle Principles and Applications.

Salman, G., Abdula, I., 1995. Development of the Mozambique and Ruvuma sedimentary basins, offshore Mozambique. Sediment. Geol. 96, 7–41. https://doi.org/10.1016/0037-0738(95)00125-R

Senanayake, I.P., Dissanayake, D.M.D.O.K., Mayadunna, B.B., Weerasekera, W.L., 2016. An approach to delineate groundwater recharge potential sites in Ambalantota, Sri Lanka using GIS techniques. Geosci. Front. 7, 115–124. https://doi.org/10.1016/j.gsf.2015.03.002

Shaban, A., Khawlie, M., Abdallah, C., 2006. Use of remote sensing and GIS to determine recharge potential zones: The case of Occidental Lebanon. Hydrogeol. J. 14, 433–443. https://doi.org/10.1007/s10040-005-0437-6

Siemann, M.G., Schramm, M., 2000. Thermodynamic modelling of the Br partition between aqueous solutions and halite. Geochim. Cosmochim. Acta 64, 1681–1693. https://doi.org/10.1016/S0016-7037(99)00385-3

Smidt, E.H., 1990. Gestão da Água Subterrânea na Ilha do Grande Maputo, Águas SubterrÂneas. Maputo.

Steinbruch, F., Weise, S.M., 2016. Characterization of the Rainfall of Central Mozambique Based on Isotopes of Water, in: Raju, N.J. (Ed.), Geostatistical and Geospatial Approaches for the Characterization of Natural Resources in the Environment. Springer International Publishing, Cham, pp. 321–325. https://doi.org/10.1007/978-3-319-18663-4_49

Steinich, B., Escolero, O., Marin, L.., 1998. Salt-water intrusion and nitrate contamination in the Valley of Hermosillo and El Sahuaral coastal aquifers, Sonora, Mexico. Hydrogeol. J. 6, 518–526.

Stigter, T.Y., Van Ooijen, S.P.J., Post, V.E.A., Appelo, C.A.J., Carvalho Dill, A.M.M., 1998. A hydrogeological and hydrochemical explanation of the groundwater composition under irrigated land in a Mediterranean environment, Algarve, Portugal. J. Hydrol. 208, 262–279. https://doi.org/10.1016/S0022-1694(98)00168-1

Stuyfzand, P.J., 1989. A new hydrochemical classification of watertypes. IAHS Publ. 182, 89–98.

Swanson, S., Bahr, J., Schwar, M., Potter, K., 2001. Two-way cluster analysis of geochemical data to constrain spring source waters. Chem Geol 179, 73–91. https://doi.org/10.1016/S0009-2541(01)00316-3

Taylor, R.G., Todd, M.C., Kongola, L., Maurice, L., Nahozya, E., Sanga, H., MacDonald, A.M., 2012. Evidence of the dependence of

groundwater resources on extreme rainfall in East Africa. Nat. Clim. Chang. 3, 374–378. https://doi.org/10.1038/nclimate1731

Thomas, B.F., Behrangi, A., Famiglietti, J.S., Behrangi@jpl, A.N., Gov, J., Famiglietti@jpl, N., Gov, J.S.F., Koch, M., Missimer, T.M., 2016. Precipitation Intensity Effects on Groundwater Recharge in the Southwestern United States. Water 8, 15. https://doi.org/10.3390/w8030090

Trabelsi, R., Zairi, M., Ben Dhia, H., 2007. Groundwater salinization of the Sfax superficial aquifer, Tunisia. 2Hydrogeology J. 15, 1341–1355.

United Nations, 2017. World Population Prospects - Population Division - United Nations [WWW Document]. World Popul. Prospect. 2017. URL https://esa.un.org/unpd/wpp/ (accessed 5.5.18).

Vandenbohede, A., Lebbe, L., 2012. Groundwater chemistry patterns in the phreatic aquifer of the central Belgian coastal plain. Appl. Geochemistry 27, 22–36. https://doi.org/10.1016/j.apgeochem.2011.08.012

Vengosh, A., Gill, J., Davisson, M.L., Hudson, G.B., 2002. A multi-isotope (B , Sr , O , H , and C) and age dating (3 H – 3 He and C) study of groundwater from Salinas Valley , California : Hydrochemistry , dynamics , and contamination processes. Warter Resour. Res. 38.

Ward, J.H., 1963. Hierarchical Grouping to Optimize an Objective Function. J. Am. Stat. Assoc. 58, 236–244. https://doi.org/10.1080/01621459.1963.10500845

Werner, A.D., Bakker, M., Post, V.E.A., Vandenbohede, A., Lu, C., Ataie-Ashtiani, B., Simmons, C.T., Barry, D.A., 2013. Seawater intrusion processes, investigation and management: Recent advances and future challenges. Adv. Water Resour. 51, 3–26. https://doi.org/10.1016/j.advwatres.2012.03.004

WHO, 2011. Guidelines for Drinking-water Quality, World Health Organization. WHO Press.

Zghibi, A., Tarhouni, J., Zouhri, L., 2013. Assessment of seawater intrusion and nitrate contamination on the groundwater quality in the Korba coastal plain of Cap-Bon (North-east of Tunisia). J. African Earth Sci. 87, 1–12. https://doi.org/10.1016/j.jafrearsci.2013.07.009